Journal of Materials Chemistry C

ROYAL SOCIETY OF CHEMISTRY

PAPER

Cite this: *J. Mater. Chem. C*, 2023, **11**, 12000

Benzothiadiazole and its derivative-based sp^2 carbon-conjugated covalent organic frameworks for photocatalytic hydrogen generation†

Chao-Qin Han, Xiaokang Sun, Xiao Liang, Lei Wang,* Hanlin Hu and Xiao-Yuan Liu *

Received 1st July 2023,
Accepted 9th August 2023

DOI: 10.1039/d3tc02305b

rsc.li/materials-c

Designing crystalline porous materials with efficient hydrogen evolution is a promising strategy to obtain green energy. Covalent organic frameworks have been regarded as outstanding photocatalysts for solar-to-hydrogen conversion. In particular, sp^2 carbon-conjugated covalent organic frameworks (sp^{2}c-COFs), *via* carbon–carbon double bond linkage, have good chemical and physical stability, which has attracted great attention in recent years. Herein, we design and synthesize two series of benzothiadiazole and its derivative-based isoreticular sp^{2}c-COFs (HIAM-0001 to HIAM-0006) for photocatalytic hydrogen generation. The experimental results show that benzothiadiazole-based COFs exhibit much higher photocatalytic activity compared with its derivative-based ones possessing much broader light-harvesting ranges. The average hydrogen evolution rates of HIAM-0001 and HIAM-0004 are up to 1410 μmol g^{-1} h^{-1} and 1526 μmol g^{-1} h^{-1} under visible-light illumination ($\lambda > 420$ nm), respectively. This work presents the relevant background for the study of the structure–property relationship in benzothiadiazole and its derivative-based sp^{2}c-COFs, and also provides a new guidance for the rational design and development of efficient photocatalysts for hydrogen generation.

Introduction

With the increasing global demand for energy and advocating the concept of sustainable development, there is no doubt that hydrogen (H_2) has been widely regarded as an ideal pollution-free green energy, which can be generated *via* photocatalytic water splitting using solar energy.[1,2] Photocatalytic hydrogen evolution technology is the simplest, mostly low cost and effective approach to obtain green energy. The most important and challenging task is to find the best photocatalysts with excellent efficiency and stability. To date, various kinds of materials have been used as photocatalysts, such as metal-oxide group compounds (*i.e.* TiO_2 and CdS),[3] polymers (*i.e.* C_3N_4[4]), quantum dots,[5] metal–organic frameworks (MOFs)[6] and so on. As one of the novel materials, covalent organic frameworks (COFs) have also been employed as catalysts for photocatalytic hydrogen generation.[7–9]

Since the first report in 2005 by Yaghi *et al.*,[10] in the last nearly twenty years, the bonding modes for preparing COFs have been developed from the initial borate and fragile ester bond to the imine bond, triazine bond, imide bond and then to the emerging olefin bond.[11] COFs have witnessed rapid development and considerable applications in fields including but not limited to catalysis,[12–14] chemical adsorption, separation and storage,[15–17] photoelectric devices,[18,19] and environment- and energy-related areas,[20–22] which can be attributed to their high stability, large specific surface areas, porosity, tunable structures and compositions. In recent years, COFs have been employed as catalysts for photocatalytic hydrogen generation.[23–26] Among these reported COFs, sp^2 carbon-conjugation COFs (sp^{2}c-COFs), with a specific topological arrangement through C=C bonds, have also been gradually explored for photocatalytic hydrogen generation.[27–31]

The first 2D sp^{2}c-COF *via* the Knoevenagel condensation reaction was reported by Feng *et al.* in 2016.[32] And then, Jiang and co-authors reported a series of sp^{2}c-COFs with different topologies, which are different from the traditional COFs, exhibiting excellent stability under various conditions.[33–35] Since then, numbers of sp^{2}c-COFs have been synthesized and applied in many fields. For example, Qiu *et al.* have reported that TFPT-BTAN-AO exhibits a high UO_2^{2+} adsorption capacity of 427 mg g^{-1} and an ultra-low detection limit of 6.2 nM for UO_2^{2+} can be achieved.[36] Jiang *et al.* reported that sp^{2}c-COFs can be used for lighting and sensing with strong fluorescence in different organic solvents, where the photoluminescence quantum yields are up to 22%, 20% and 18% for sp^{2}c-COF,

Hoffmann Institute of Advanced Materials, Shenzhen Polytechnic, 7098 Liuxian Blvd, Nanshan District, Shenzhen, 518055, P. R. China.
E-mail: wlhiam@szpt.edu.cn, liuxiaoyuan1989@szpt.edu.cn

† Electronic supplementary information (ESI) available. See DOI: https://doi.org/10.1039/d3tc02305b

sp^2c-COF-2 and sp^2c- COF-3 in water.[37] Feng and co-authors synthesized a two-dimensional CCP-HATN, which can be hybridized with carbon nanotubes to exhibit a high capacity of 116 mA h g^{-1} with excellent cycling stability and rate capability, indicative of its potential application as an excellent organic cathode material for lithium-ion batteries.[38] Wang *et al.* designed and synthesized a 2D Por-sp^2c-COF with excellent chemical stability in strong acids and bases, which can be used as a metal-free heterogeneous photocatalyst for the visible-light-induced aerobic oxidation of amines to imines with high reusability and photocatalytic performance.[39] Besides these aforementioned applications, Liu *et al.* synthesized sp^2c- and imine-linked COFs using a three-component synthesis method, which exhibits higher hydrogen production activity compared with two-component COFs.[7]

Benzothiadiazole is one of the representative electron-deficient groups and has been widely used to synthesize frameworks, such as COFs[40–45] and metal–organic frameworks (MOFs).[46] For example, benzothiadiazole-based 2D imine-linked COFs were reported by Liu *et al.* as efficient heterogeneous photocatalysts for organic transformation under visible light.[47] Chen and co-workers presented that the substitution groups on the benzothiadiazole moiety have significant effects on their performances of photocatalytic hydrogen generation.[42,44] Although great efforts have been made to prepare benzothiadiazole-based COFs and explore their potential applications, nevertheless, there is a lack of systematic study about the light-harvesting range and the photocatalytic performance relationship using benzothiadiazole and its derivative-based COFs, especially for sp^2c-COFs.

Our group has reported a series of benzothiadiazole and its derivative-based MOFs with tunable emission and absorption properties, which can be used as ideal platforms for energy transfer and sensing.[46,48–50] However, rare works have been done to construct sp^2c-COFs using benzothiadiazole and its derivatives as the building units to systematically tune the optical behaviors and explore the corresponding influence on photocatalytic activity. Bearing the aforementioned consideration in mind, we envision that benzothiadiazole and its derivative based sp^2c-COFs might be synthesized with tunable optical properties, which can be used as an ideal platform to study the structure–property relationship for photocatalytic hydrogen generation. Herein, we synthesize six benzothiadiazole and its derivative based sp^2c-COFs (HIAM-0001 to HIAM-0006, HIAM = Hoffmann Institute of Advanced Materials) with tunable light absorption behaviors and explore their application for photocatalytic hydrogen generation. Our work revealed that although HIAM-0004 possesses a much less light-absorption range compared with HIAM-0003 and HIAM-0006, it shows much higher photocatalytic H_2 evolution, indicating that the light absorption range is not directly proportional to the photocatalytic activity.

Results and discussion

Synthesis and characterization of benzothiadiazole and its derivative-based sp^2c-COFs

Benzothiadiazole (BT) and its two derivatives, benzoselenadiazole (BS) and naphthothiadiazole (NT), with gradually increased electron-withdrawing capacity were chosen as the acceptor groups. Then, the three corresponding compounds, 5′,5′′′′-(benzo[*c*][1,2,5]thiadiazole-4,7-diyl)bis(([1,1′:3′,1″-terphenyl]-4,4″-dicarbaldehyde)) (BT-TDA), 5′,5′′′′-(benzo[*c*][1,2,5]selenadiazole-4,7-diyl)-bis(([1,1′:3′,1″-terphenyl]-4,4″-dicarbaldehyde)) (BS-TDA) and 5′,5′′′′-(naphtho[2,3-*c*][1,2,5]thiadiazole-4,9-diyl)bis(([1,1′:3′,1″-terphenyl]-4,4″-dicarbaldehyde)) (NT-TDA), were synthesized *via* the Suzuki–Miyaura coupling reaction. These three organic building units were then employed as monomers to react with 2,2′-(1,4-phenylene)diacetonitrile (PDAN) *via* the Knoevenagel condensation reaction under solvothermal conditions to obtain three sp^2c-COFs, HIAM-0001 to HIAM-0003 (Fig. 1a). To achieve a highly crystalline COF sample, we optimized the reaction parameters including the molar ratio between monomers, solvent combinations, the amount of the base catalyst and the reaction temperature (Table S1, ESI†). The optimal condensation reaction for HIAM-0001 was conducted in anisole/EtOH (1/1, 1 mL) and tetrabutylammonium hydroxide (TBAH, 25% in menthol, 60 μL) at 120 °C for three days. HIAM-0002 was obtained using the same solvent combination as HIAM-0001, but using 40 μL of TBAH at 150 °C for three days. The synthesis method for HIAM-0003 to achieve excellent crystallinity was the same as that for HIAM-0001, except for using different molar ratios for two monomers. HIAM-0001 is the same as sp^2c-COF-10,35 which possesses a hexagon topology with a 2D layered packing structure and 1D tetragonal channels as shown in Fig. 1b and c. Powder X-ray diffraction (PXRD) analyses clearly elucidated the high crystallinity and the isoreticular nature of the as-synthesized HIAM-0001, HIAM-0002 and HIAM-0003 (Fig. 1d). Beyond this, synchrotron small-angle X-ray scattering (SAXS) patterns also proved the good crystallinity of these three sp^2c-COFs (Fig. 1d inset). The Pawley refined pattern can well reproduce the experimental PXRD pattern with only small differences (R_{wp} = 5.58% and R_p = 3.66% for HIAM-0001, R_{wp} = 6.52% and R_p = 4.33% for HIAM-0002, R_{wp} = 6.48% and R_p = 3.98% for HIAM-0003) (Fig. S1, ESI†). Fourier transform infrared (FT-IR) spectra of the obtained COFs were executed as shown in Fig. S2 (ESI†). The characteristic peaks of aldehyde C–H stretching in BT-TDA (2725 cm^{-1}) and C≡N stretching in PDAN (2250 cm^{-1}) were not detected. The C=O stretching vibration of BT-TDA at 1690 cm^{-1} decreased while the C=C stretching vibration at 1591 cm^{-1} increased accompanying with the appearance of a new peak at 2220 cm^{-1}, which was assigned to the C≡N stretching in the vinyl cyano group for HIAM-0001. The same phenomena were also observed in HIAM-0002 and HIAM-0003. Furthermore, this result was supported by the ^{13}C solid-state NMR spectroscopic data (Fig. S3, ESI†). The formation of C=C bonds *via* the Knoevenagel condensation reaction was confirmed by characteristic peaks at 106 ppm, 107 ppm and 107 ppm for HIAM-0001, HIAM-0002 and HIAM-0003, respectively, which can be ascribed to the carbon of the cyano group. Together, these results indicated the successful synthesis of sp^2-carbon conjugated HIAM-0001, HIAM-0002 and HIAM-0003. The morphological features of the as-synthesized COFs were characterized using scanning electron microscopy (SEM) (Fig. S4, ESI†). SEM images indicated that HIAM-0001, HIAM-0002 and

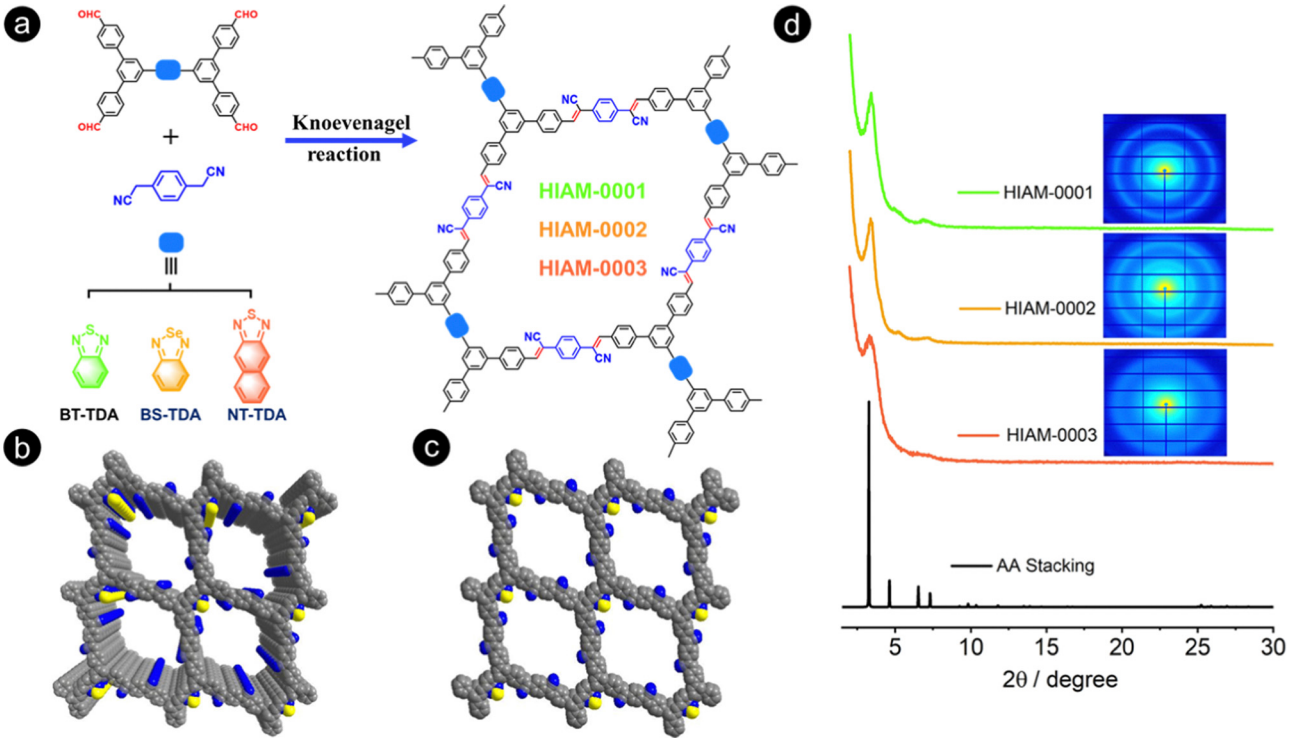

Fig. 1 (a) Synthesis scheme for HIAM-0001, HIAM-0002 and HIAM-0003. Crystal structures of multi-layered (b) and one-layered (c) HIAM-0001 adopted from sp^{2}c-COF-10. (d) Experimental and simulated PXRD patterns of HIAM-0001, HIAM-0002, HIAM-0003 and sp^{2}c-COF-10 (inset: SAXS scattering pattern).

HIAM-0003 present rod-like shapes. The elemental compositions of COFs were probed by energy dispersive X-ray spectroscopy (EDS). HIAM-0001 and HIAM-0003 clearly show a homogeneous distribution of C, N, and S elements, while HIAM-0002 exhibits a uniform distribution of C, N and Se elements (Fig. S5, ESI†).

To further extend the structures of benzothiadiazole and its derivative-based sp^{2}c-COFs, we further synthesized three isoreticular expansions of HIAM-0001, HIAM-0002 and HIAM-0003 to obtain HIAM-0004, HIAM-0005 and HIAM-0006 using 2,2′-([2,2′-bipyridine]-5,5′-diyl)diacetonitrile (BPyDAN) as the second building unit (Fig. 2a). As expected, the PXRD patterns of HIAM-0004 to HIAM-0006 revealed that the three COFs also disclosed excellent crystallinity and isoreticular nature, where the characteristic diffraction peak at 2.96° (110) is consistent with the previously reported sp^{2}c-COF-14.[35] Similarly, SXAS scattering experiments also disclosed excellent crystallinity of three sp^{2}c-COFs (Fig. 2b inset). The Pawley refinement patterns were obtained for HIAM-0004, HIAM-0005 and HIAM-0006, which agreed well with the experimental results (Fig. S6, ESI†). Taking HIAM-0004 as the model sample as shown in Fig. 2c and d, the crystal topology structure is identical to HIAM-0001. From the PXRD patterns, HIAM-COFs with an AA-stacking mode can be observed. FT-IR spectra indicated that no C≡N stretching from BPyDAN (2255 cm^{-1}) was recorded in three COFs. However, new characteristic peaks from the C≡N stretching in the vinyl cyano group appeared at 2215 cm^{-1}, 2210 cm^{-1} and 2215 cm^{-1} for HIAM-0004, HIAM-0005 and HIAM-0006, respectively (Fig. S7, ESI†). Additionally, solid-state ^{13}C NMR data indicated that characteristic peaks appeared at 105 ppm, 105 ppm and 104 ppm (Fig. S8, ESI†). These aforementioned results demonstrated the successful synthesis of HIAM-0004, HIAM-0005 and HIAM-0006. SEM images also revealed the rod-like morphology of these three COFs (Fig. S9, ESI†). EDS confirmed the uniform distribution of elements in the formed COFs (Fig. S10, ESI†).

Besides, the thermal stability of sp^{2}c-COFs was evaluated by the thermogravimetric analysis (TGA), where HIAM-0001, HIAM-0002 and HIAM-0003 were stable up to 400 °C, and they can maintain more than half weight when heated up to 800 °C (Fig. S11, ESI†). Similar phenomena can also be observed in HIAM-0004, HIAM-0005 and HIAM-0006 (Fig. S12, ESI†), revealing that sp^{2}c-COFs have distinct thermal stability. Moreover, the chemical stability of sp^{2}c-COFs was further investigated. HIAM-0001 and HIAM-0002 were selected as representative samples to carry out the robustness of sp^{2}c-COFs. The two samples remain the long-range order and chemical compositions after soaking in boiling water and aqueous solutions of hydrochloric acid (12 M and 6 M) and sodium hydroxide (0.05 M) for 24 hours, as confirmed by PXRD and FT-IR spectroscopy (Fig. S13, ESI†). These results indicate that sp^{2}c-COFs possess excellent thermal and chemical stability.

Optical properties of HIAM-0001 to HIAM-0006

The steady-state photoluminescence (PL) spectra were recorded for these six sp^{2}c-COFs to investigate benzothiadiazole and its derivative-induced differences in optical behaviors. As depicted

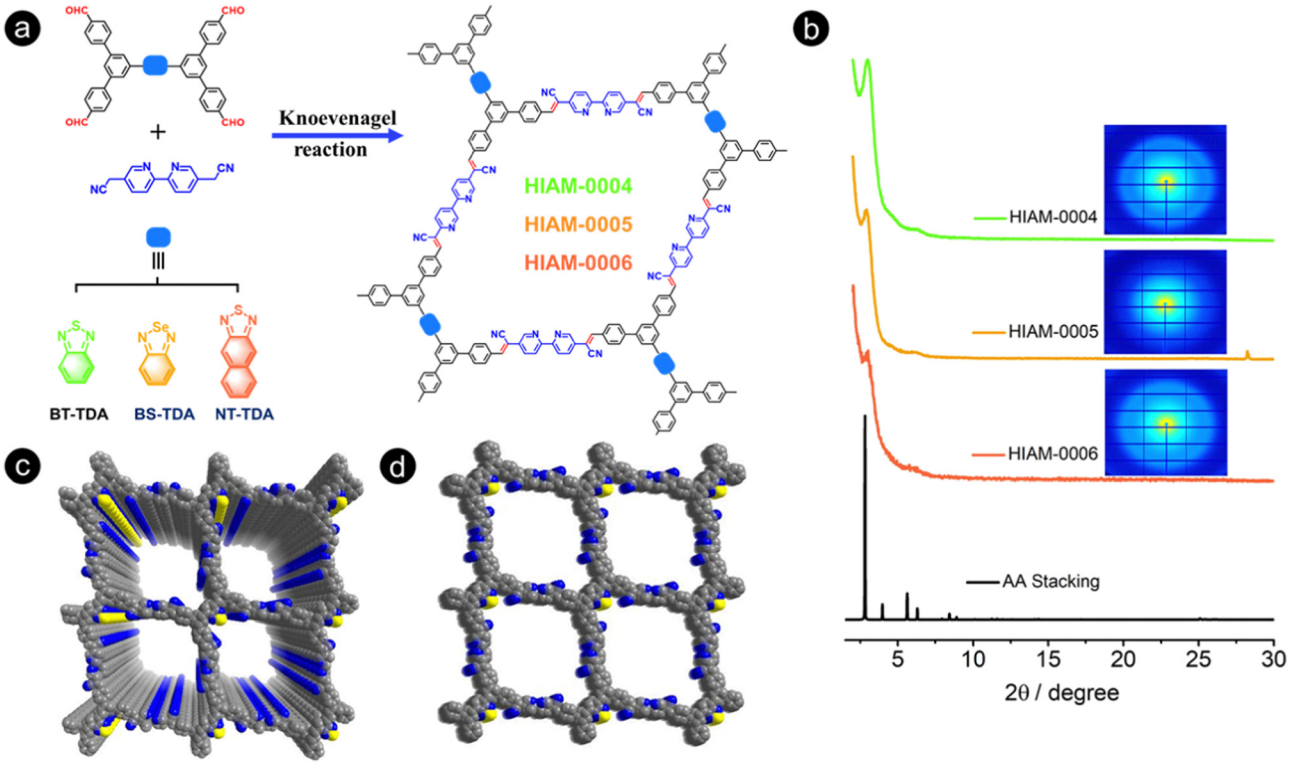

Fig. 2 (a) Synthesis scheme for HIAM-0004, HIAM-0005 and HIAM-0006. (b) Experimental and simulated PXRD patterns of HIAM-0004, HIAM-0005, HIAM-0006 and sp^{2}c-COF-14 (inset: SAXS scattering pattern). Crystal structures of multi-layered (c) and one-layered (d) HIAM-0004 adopted from sp^{2}c-COF-14.

in Fig. 3a and d, the maximum emission peaks appear at 565, 565, 630, 560, 566 and 637 nm for HIAM-0001, HIAM-0002, HIAM-0003, HIAM-0004, HIAM-0005 and HIAM-0006, respectively. The result indicated that replacing a S atom on BT-TDA of HIAM-0001 or HIAM-0004 with a Se atom to obtain HIAM-0002 and HIAM-0005 has no significant effect on the emission behaviors. While, a larger emission red-shift can be observed in constructed MOFs when replacing the S atom with the Se atom in the organic linker.[46,49] We envision that the S and Se atoms causing emission differences might be remarkably restricted in 2D COF structures. However, compared with HIAM-0001 and HIAM-0002, a 65 nm bathochromic-shift was recorded for HIAM-0003, which can be ascribed to the much stronger electron-withdrawing capacity of naphthothiadiazole compared with benzothiadiazole and benzoselenadiazole, consistent with that we observed in the MOF.[46] Similar emission behavior was also observed in HIAM-0006. For a better understanding of fluorescent behavior, corresponding optical images of sp^{2}c-COFs under 365 nm excitation were obtained as shown in Fig. S14 and S15 (ESI†), in which the emission colors of six COFs were well consistent with corresponding maximum emission wavelengths.

It is well known that benzothiadiazole and its derivatives have strong electron-withdrawing capacity, and the inherent electronic absorption features were further explored by solid-state electronic UV-vis reflectance spectroscopy. As shown in Fig. 3b and e, HIAM-0003 and HIAM-0006 exhibit much broader light-absorption ranges compared with the other four COFs, with absorption edges up to approximately 600 nm. This result demonstrates that much strong light-harvesting can be achieved using acceptor groups with strong electron-withdrawing capacity in donor–acceptor–donor type building units. Moreover, we found that there was no obvious effect on the light absorption and emission behavior of sp^{2}c-COFs after replacing phenyl with bipyridinyl, which indicates that the optical behaviors are governed by benzothiadiazole and its derivative-based units. Then, the optical bandgap energies (Eg) of HIAM-0001, HIAM-0002, HIAM-0003, HIAM-0004, HIAM-0005 and HIAM-0006 were calculated to be 2.53, 2.49, 2.10, 2.50, 2.46 and 2.10 eV, respectively, based on Tauc's plots (Fig. 3c and f). Furthermore, the energy levels of these sp^{2}c-COFs are obtained according to Mott–Schottky plots (Fig. S16 and S17, ESI†), where the positive slopes indicated the n-type semiconductor nature of these sp^{2}c-COFs. The flat band minimum positions of HIAM-0001, HIAM-0002, HIAM-0003 HIAM-0004, HIAM-0005 and HIAM-0006 are −0.93, −0.97, −1.03, −0.91, −0.95 and −1.00 V *vs.* the normal hydrogen electrode (NHE, pH 6.8), respectively (Fig. 4a). Given the match energy levels of these sp^{2}c-COFs and that for water splitting, we believe that these COFs might be suitable for photocatalytic hydrogen generation.

Performance of photocatalytic hydrogen generation

Encouraged by the aforementioned results, the photocatalytic hydrogen evolution performances of sp^{2}c-COFs were investigated from water under visible light irradiation (Xe lamp 300 W, $\lambda > 420$ nm) in the presence of H_2PtCl_6 as the precursor

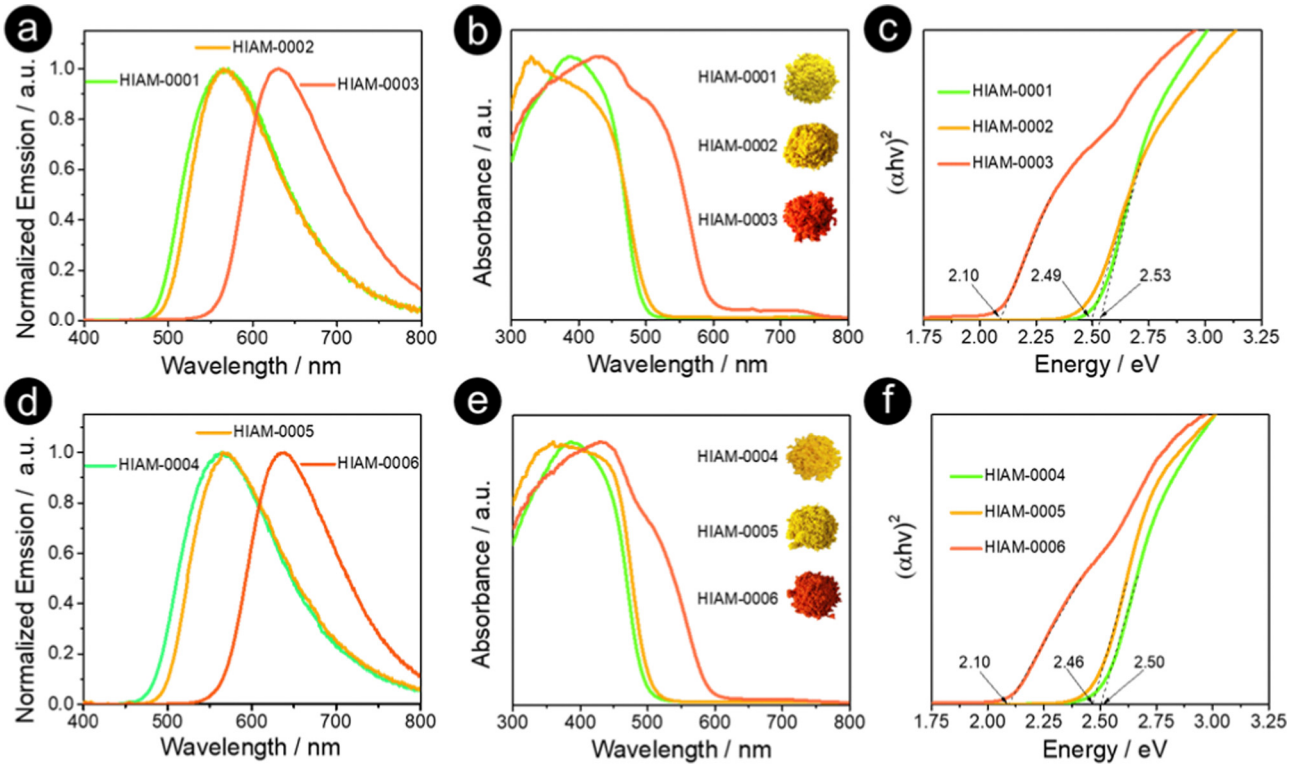

Fig. 3 Normalized solid-state emission (a) and absorption (b) spectra and Tauc plots (c) of HIAM-0001, HIAM-0002 and HIAM-0003. Normalized solid-state emission (d) and absorption (e) spectra and Tauc plots (f) of HIAM-0004, HIAM-0005 and HIAM-0006. The inserted photographs in (b) and (e) show the colors of HIAM-0001 to HIAM-0006.

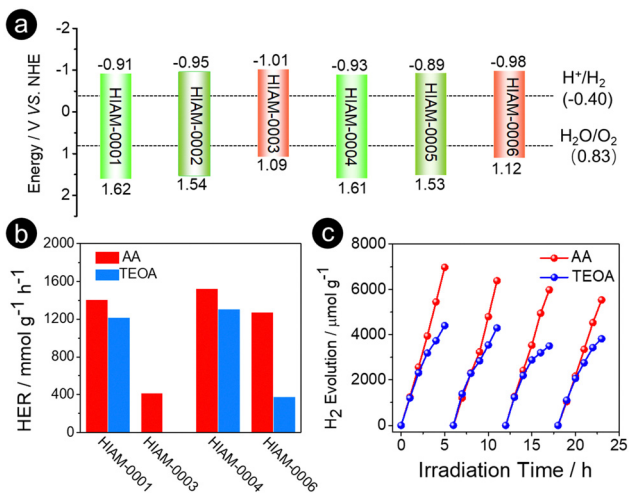

Fig. 4 (a) Schematic energy band structures of HIAM-0001, HIAM-0002, HIAM-0003, HIAM-0004, HIAM-0005 and HIAM-0006. (b) Photocatalytic H_2 evolution rates of HIAM-0001, HIAM-0003, HIAM-0004 and HIAM-0006. (c) Long-term H_2 production of HIAM-0001.

of the co-catalyst. The control experiments indicated the necessity of visible light, sacrificial agents, co-catalysts and COFs for efficient photocatalytic hydrogen evolution (Fig. S18, ESI†). We carried out the effect of the photo-deposited Pt content on the hydrogen production activity using different electron donors (Fig. S19, ESI†). For example, 10 mg of HIAM-0001 mixed with 3 wt% Pt in the presence of triethanolamine (TEOA) (25 vol%) as the sacrificial reagent in water (50 mL), the system exhibited a hydrogen evolution rate (HER) of 160 μmol g^{-1} h^{-1} under visible-light irradiation ($\lambda > 420$ nm). Furthermore, when the amount of photo-deposited Pt was increased to 12 wt%, the HER dramatically increased to 1217 μmol g^{-1} h^{-1}. When ascorbic acid (AA) (0.1 M) was used as the sacrificial reagent, the hydrogen evolution of HIAM-0001 first increased and then decreased with the increasing photo-deposited Pt content, where the highest average HER of 1410 μmol g^{-1} h^{-1} was achieved using 5 wt% Pt. As shown in Fig. 4b, under the optimized conditions, different photocatalytic hydrogen generation activities were observed for these six sp^2c-COFs. It should be noted that no hydrogen was generated using HIAM-0002 and HIAM-0004 as photocatalysts, which might be ascribed to the fact that benzoselenadiazole-based COFs will quickly decompose under the reaction conditions. The higher HER was realized using benzothiadiazole-based COFs, HIAM-0001 and HIAM-0004, especially using AA as the electron donor. Although HIAM-0003 and HIAM-0006 exhibit broader light-harvesting ranges compared with HIAM-0001 and HIAM-0004, the HERs of HIAM-0003 and HIAM-0006 are much lower than those of HIAM-0001 and HIAM-0004. HIAM-0004 exhibited the superior HER up to 1526 μmol g^{-1} h^{-1} among these six sp^2c-COFs. These results demonstrate that the only extended light-absorption range is not enough to enhance the HER, which should be evaluated and optimized with the electronic structures and other physical

properties of photocatalysts to realize high efficiency for photocatalytic hydrogen generation.[51]

Beyond this, we recorded transmission electron microscopy (TEM) and X-ray photoelectron (XPS) spectra to confirm the formation of Pt NPs in photocatalytic water splitting. The TEM images indicated that Pt nanoparticles with spherical shapes were generated in the process of photocatalytic hydrogen generation (Fig. S20, ESI†). Simultaneously, the XPS data also confirmed the above result (Fig. S21, ESI†), in which the Pt 4f XPS spectra revealed the coexistence of Pt^0 and Pt^{2+}, and the proportion of Pt^0 was higher than that of Pt^{2+}. On the other hand, the Brunauer–Emmett–Teller (BET) surface areas of HIAM-001, HIAM-003, HIAM-004 and HIAM-006 were calculated to be 511, 384, 397 and 482 $m^2\ g^{-1}$, respectively, and the pore size distributions were obtained stemming from the nonlocal density functional theory (NLDFT) model from the nitrogen isotherm (Fig. S22, ESI†). No direct correlation can be found between the surface area and the efficiency of photocatalytic hydrogen generation for these COFs. To further explore the phenomenon, electrochemical impedance spectroscopy was performed (Fig. S23, ESI†). The experiments show that the semicircles of HIAM-0001 and HIAM-0004 are smaller than those of HIAM-0003 and HIAM-0006, indicating faster charge separation for the former sp^2c-COFs; thus, to some extent, an enhanced photocatalytic activity was obtained. Additionally, reactive oxygen species were obtained for HIAM-0004 under irradiation and confirmed by the electron paramagnetic resonance (EPR) spectra. The distinct EPR signals corresponding to $^1O_2$ and $^\bullet O_2^-$ were observed after irradiation while no signals appeared under the dark conditions (Fig. S24, ESI†).

Furthermore, we carried out the long-time performance test under the optimized photocatalytic conditions using HIAM-0001 as shown in Fig. 4c. Slightly decreased activity was observed with increased cycles, which can be assigned to the partial loss of COF samples during the recovery process. The apparent quantum yield (AQY) was measured to be 0.49% for HIAM-0004 under optimized conditions, which is comparable to those previously reported for 2D sp^2c-COFs.[52] The almost identical SEM images, FT-IR spectra and PXRD patterns of HIAM-0001, HIAM-4003, HIAM-0004 and HIAM-0006 before and after catalysis demonstrate their excellent stability under reaction conditions (Fig. S25–S29, ESI†).

Many works have been done to construct COFs using benzothiadiazole-based building units, where some of them have been used as photocatalysts for hydrogen generation, especially for imine-based COFs. The sp^2c-COFs in the present work exhibit comparable efficiency for photocatalytic hydrogen evolution with some imine-linked COFs as summarized in Table S2 (ESI†), which provides a research basis for benzothiadiazole-based COFs for hydrogen evolution from water.

Conclusions

In conclusion, we have designed and synthesized two series of benzothiadiazole and its derivative-based isoreticular sp^2 carbon-conjugated covalent organic frameworks (sp^2c-COFs). The chemical–physical properties of six sp^2c-COFs were systematically studied to build the structure–performance relationship for photocatalytic hydrogen generation. The results revealed that benzothiadiazole-based COFs exhibit much higher photocatalytic activity compared with its derivative-based ones. It is important to extend the light-absorption ranges of photo-catalysts, while it is not the only factor to determine the photocatalytic efficiency of resultant COFs. This work not only provides the relevant knowledge for the study of benzothiadiazole and its derivative-based sp^2c-COFs, but also shed light on the rational designing and constructing COFs with high performances for photocatalytic hydrogen generation.

Conflicts of interest

There are no conflicts to declare.

Acknowledgements

X.-Y. Liu acknowledges the financial support from start-up funding for Shenzhen High-Caliber Personnel of Shenzhen Polytechnic (6022310053K).

References

1 T. Su, Q. Shao, Z. Qin, Z. Guo and Z. Wu, *ACS Catal.*, 2018, **8**, 2253–2276.
2 H. Wang, L. Zhang, Z. Chen, J. Hu, S. Li, Z. Wang, J. Liu and X. Wang, *Chem. Soc. Rev.*, 2014, **43**, 5234–5244.
3 L. Shang, B. Tong, H. Yu, G. I. N. Waterhouse, C. Zhou, Y. Zhao, M. Tahir, L.-Z. Wu, C.-H. Tung and T. Zhang, *Adv. Energy Mater.*, 2016, **6**, 1501241.
4 Q. Zhu, Z. Xu, B. Qiu, M. Xing and J. Zhang, *Small*, 2021, **17**, 2101070.
5 H. Su, W. Wang, R. Shi, H. Tang, L. Sun, L. Wang, Q. Liu and T. Zhang, *Carbon Energy*, 2023, e280.
6 Y. He, T. Lv, B. Xiao, B. Liu, T. Zhou, J. Zhang, Y. Zhang, G. Zhang and Q. Liu, *J. Mater. Chem. C*, 2023, **11**, 6800–6818.
7 Z. Li, T. Deng, S. Ma, Z. Zhang, G. Wu, J. Wang, Q. Li, H. Xia, S. W. Yang and X. Liu, *J. Am. Chem. Soc.*, 2023, **145**, 8364–8374.
8 R. Chen, Y. Wang, Y. Ma, A. Mal, X.-Y. Gao, L. Gao, L. Qiao, X.-B. Li, L.-Z. Wu and C. Wang, *Nat. Commun.*, 2021, **12**, 1354.
9 S. Wei, F. Zhang, W. Zhang, P. Qiang, K. Yu, X. Fu, D. Wu, S. Bi and F. Zhang, *J. Am. Chem. Soc.*, 2019, **141**, 14272–14279.
10 A. P. Cote, A. I. Benin, N. W. Ockwig, M. O'Keeffe, A. J. Matzger and O. M. Yaghi, *Science*, 2005, **310**, 1166–1170.
11 M. S. Lohse and T. Bein, *Adv. Funct. Mater.*, 2018, **28**, 1705553.
12 H. Chen, H. S. Jena, X. Feng, K. Leus and P. V. D. Voort, *Angew. Chem., Int. Ed.*, 2022, **61**, e202204938.
13 X. Zhao, P. Pachfule, S. Li, T. Langenhahn, M. Ye, C. Schlesiger, S. Praetz, J. Schmidt and A. Thomas, *J. Am. Chem. Soc.*, 2019, **141**, 6623–6630.
14 Y. Qian, Y. Han, X. Zhang, G. Yang, G. Zhang and H. L. Jiang, *Nat. Commun.*, 2023, **14**, 3083.
15 C. Wang, Y. Wang, R. Ge, X. Song, X. Xing, Q. Jiang, H. Lu, C. Hao, X. Guo, Y. Gao and D. Jiang, *Chem. – Eur. J.*, 2018, **24**, 585–589.

16 S. S. Han, H. Furukawa, O. M. Yaghi and W. A. Goddard, *J. Am. Chem. Soc.*, 2008, **130**, 11580–11581.
17 P. Wang, Q. Xu, Z. Li, W. Jiang, Q. Jiang and D. Jiang, *Adv. Mater.*, 2018, **30**, 1801991.
18 S. Yang, D. Streater, C. Fiankor, J. Zhang and J. Huang, *J. Am. Chem. Soc.*, 2021, **143**, 1061–1068.
19 S. Haldar, D. Chakraborty, B. Roy, G. Banappanavar, K. Rinku, D. Mullangi, P. Hazra, D. Kabra and R. Vaidhyanathan, *J. Am. Chem. Soc.*, 2018, **140**, 13367–13374.
20 B. P. Biswal, H. A. Vignolo-González, T. Banerjee, L. Grunenberg, G. Savasci, K. Gottschling, J. Nuss, C. Ochsenfeld and B. V. Lotsch, *J. Am. Chem. Soc.*, 2019, **141**, 11082–11092.
21 X. Wang, L. Chen, S. Y. Chong, M. A. Little, Y. Wu, W. H. Zhu, R. Clowes, Y. Yan, M. A. Zwijnenburg, R. S. Sprick and A. I. Cooper, *Nat. Chem.*, 2018, **10**, 1180–1189.
22 S. Ghosh, A. Nakada, M. A. Springer, T. Kawaguchi, K. Suzuki, H. Kaji, I. Baburin, A. Kuc, T. Heine, H. Suzuki, R. Abe and S. Seki, *J. Am. Chem. Soc.*, 2020, **142**, 9752–9762.
23 T. Banerjee, K. Gottschling, G. Savasci, C. Ochsenfeld and B. V. Lotsch, *ACS Energy Lett.*, 2018, **3**, 400–409.
24 P. Pachfule, A. Acharjya, J. Roeser, T. Langenhahn, M. Schwarze, R. Schomacker, A. Thomas and J. Schmidt, *J. Am. Chem. Soc.*, 2018, **140**, 1423–1427.
25 W. Huang, Q. He, Y. Hu and Y. Li, *Angew. Chem., Int. Ed.*, 2019, **58**, 8676–8680.
26 C. Li, J. Liu, H. Li, K. Wu, J. Wang and Q. Yang, *Nat. Commun.*, 2022, **13**, 2357.
27 X. Li, *Mater. Chem. Front.*, 2021, **5**, 2931–2949.
28 T. He, K. Geng and D. Jiang, *Trends Chem.*, 2021, **3**, 431–444.
29 S. Li, L. Li, Y. Li, L. Dai, C. Liu, Y. Liu, J. Li, J. Lv, P. Li and B. Wang, *ACS Catal.*, 2020, **10**, 8717–8726.
30 S. Ma, T. Deng, Z. Li, Z. Zhang, J. Jia, G. Wu, H. Xia, S. W. Yang and X. Liu, *Angew. Chem., Int. Ed.*, 2022, **61**, e202208919.
31 L. Dai, A. Dong, X. Meng, H. Liu, Y. Li, P. Li and B. Wang, *Angew. Chem., Int. Ed.*, 2023, **62**, e202300224.
32 X. Zhuang, W. Zhao, F. Zhang, Y. Cao, F. Liu, S. Bi and X. Feng, *Polym. Chem.*, 2016, **7**, 4176–4181.
33 E. Jin, M. Asada, Q. Xu, S. Dalapati, M. A. Addicoat, M. A. Brady, H. Xu, T. Nakamura, T. Heine, Q. Chen and D. Jiang, *Science*, 2017, **357**, 673–676.
34 D. Jiang, *Chem*, 2020, **6**, 2461–2483.
35 E. Jin, K. Geng, S. Fu, M. A. Addicoat, W. Zheng, S. Xie, J.-S. Hu, X. Hou, X. Wu, Q. Jiang, Q.-H. Xu, H. I. Wang and D. Jiang, *Angew. Chem., Int. Ed.*, 2022, **61**, e202115020.
36 W.-R. Cui, C.-R. Zhang, W. Jiang, F.-F. Li, R.-P. Liang, J. Liu and J.-D. Qiu, *Nat. Commun.*, 2020, **11**, 436.
37 E. Jin, J. Li, K. Geng, Q. Jiang, H. Xu, Q. Xu and D. Jiang, *Nat. Commun.*, 2018, **9**, 4143.
38 S. Xu, G. Wang, B. P. Biswal, M. Addicoat, S. Paasch, W. Sheng, X. Zhuang, E. Brunner, T. Heine, R. Berger and X. Feng, *Angew. Chem., Int. Ed.*, 2019, **58**, 849–853.
39 R. Chen, J.-L. Shi, Y. Ma, G. Lin, X. Lang and C. Wang, *Angew. Chem., Int. Ed.*, 2019, **58**, 6430–6434.
40 Y. He, G. Liu, Z. Liu, J. Bi, Y. Yu and L. Li, *ACS Energy Lett.*, 2023, **8**, 1857–1863.
41 S. Bhunia, A. Pena-Duarte, H. Li, H. Li, M. F. Sanad, P. Saha, M. A. Addicoat, K. Sasaki, T. A. Strom, M. J. Yacaman, C. R. Cabrera, R. Seshadri, S. Bhattacharya, J. L. Bredas and L. Echegoyen, *ACS Nano*, 2023, **17**, 3492–3505.
42 J. N. Chang, Q. Li, J. W. Shi, M. Zhang, L. Zhang, S. Li, Y. Chen, S. L. Li and Y. Q. Lan, *Angew. Chem., Int. Ed.*, 2023, **63**, e202218868.
43 C. Lin, X. Liu, B. Yu, C. Han, L. Gong, C. Wang, Y. Gao, Y. Bian and J. Jiang, *ACS Appl. Mater. Interfaces*, 2021, **13**, 27041–27048.
44 W. Chen, L. Wang, D. Mo, F. He, Z. Wen, X. Wu, H. Xu and L. Chen, *Angew. Chem., Int. Ed.*, 2020, **59**, 16902–16909.
45 Z. Zhao, Y. Zheng, C. Wang, S. Zhang, J. Song, Y. Li, S. Ma, P. Cheng, Z. Zhang and Y. Chen, *ACS Catal.*, 2021, **11**, 2098–2107.
46 S. Wu, D. Ren, K. Zhou, H. L. Xia, X. Y. Liu, X. Wang and J. Li, *J. Am. Chem. Soc.*, 2021, **143**, 10547–10552.
47 Z. Li, Y. Zhi, P. Shao, H. Xia, G. Li, X. Feng, X. Chen, Z. Shi and X. Liu, *Appl. Catal., B*, 2019, **245**, 334–342.
48 H. L. Xia, K. Zhou, S. Wu, D. Ren, K. Xing, J. Guo, X. Wang, X. Y. Liu and J. Li, *Chem. Sci.*, 2022, **13**, 8036–8044.
49 D. Ren, H.-L. Xia, K. Zhou, S. Wu, X.-Y. Liu, X. Wang and J. Li, *Angew. Chem., Int. Ed.*, 2021, **60**, 25048–25054.
50 H. L. Xia, K. Zhou, J. Guo, J. Zhang, X. Huang, D. Luo, X. Y. Liu and J. Li, *Chem. Sci.*, 2022, **13**, 9321–9328.
51 M. Kou, Y. Wang, Y. Xu, L. Ye, Y. Huang, B. Jia, H. Li, J. Ren, Y. Deng, J. Chen, Y. Zhou, K. Lei, L. Wang, W. Liu, H. Huang and T. Ma, *Angew. Chem., Int. Ed.*, 2022, **61**, e202200413.
52 E. Jin, Z. Lan, Q. Jiang, K. Geng, G. Li, X. Wang and D. Jiang, *Chem*, 2019, **5**, 1632–1647.

